Science and Technology Indonesia
e-ISSN:2580-4391 *p*-ISSN:2580-4405
Vol. 8, No. 4, October 2023

Research Paper

One-pot Hydrothermal Synthesis and Characterization of Zirconium Oxide Nanoparticles

Suresh Sagadevan[1,3], Jayasingh Anita Lett[2], Is Fatimah[3*]

[1]*Nanotechnology & Catalysis Research Centre, University of Malaya, Kuala Lumpur, 50603, Malaysia*
[2]*Department of Physics, Sathyabama Institute of Science and Technology, Chennai, 600119, India*
[3]*Department of Chemistry, Faculty of Mathematics and Natural Sciences, Universitas Islam Indonesia, Kampus Terpadu UII, Jl. Kaliurang Km 14, Sleman, Yogyakarta, 55584, Indonesia*
***Corresponding author**: isfatimah@uii.ac.id

Abstract
Zirconia (also known as zirconium dioxide, ZrO_2) is a white crystalline naturally occurring mineral that offers excellent optical, dielectric, and mechanical properties. Considering these properties and referring to previous studies on the optimization of ZrO_2 NPs synthesis, in the present study, we studied the crystalline, optical, and fluorescence properties of ZrO_2 nanoparticles (NPs) formed by the hydrothermal synthesis route. The physicochemical features of the nanoparticles were examined in the photocatalytic oxidation of rhodamine B. From the powder XRD analysis, the ZrO_2 NPs were found to be highly crystalline, while the fluorescence (FL) spectra indicated an emission band at 473 nm, which could be linked to a blue shift. Also, the FTIR and Raman spectroscopies confirmed the functionality and bonding, and in addition, the XPS analysis provided the elemental peaks of Zr 3d and O 1s, where all these analyses evidenced the successful formation of ZrO_2. Examination of the photocatalytic activity of ZrO_2 NPs revealed the capability of the material for rhodamine B photocatalytic degradation effectively, with a degradation efficiency of 86% after 2 h of treatment. Moreover, the nanoparticles exhibited stability and reusability over five cycles. Overall, from the analysis, ZrO_2 NPs can be easily formed via the hydrothermal route with tailored optical and fluorescence properties to find applications in the electronics industry for the manufacturing of light-emitting devices.

Keywords
Zirconia, Hydrothermal Synthesis, Optical Properties, Fluorescence Spectra, Raman Spectrum

Received: 16 May 2023, Accepted: 28 July 2023
https://doi.org/10.26554/sti.2023.8.4.585-593

1. INTRODUCTION

Zirconia or zirconium dioxide (ZrO_2) is a naturally available inert material which has great technological importance in the non-metallic and dental ceramics category because of the natural colour, crystallinity, high mechanical strength, chemical and biological stabilities, resistance from corrosion and microbial attack, etc.(Lebeau et al., 2020; Tran et al., 2022). This material possesses wide bandgaps in the range of 3 to 7 eV (depending on its crystal phase of cubic, tetragonal, and monoclinic), which is similar to any p-type semiconductor material and hence maintains the capacity to display ample oxygen vacancies followed by the irradiation (Li et al., 2017). The availability or capacity of ZrO_2 to generate defective oxygen sites (high k-gate dielectric) additionally favors for high oxygen ion conductivity and redox ability, thereby making it a very useful ingredient in the catalysis and sensor-related applications which includes the solid oxide fuel cells, optical coatings, nitrogen oxide, and oxygen sensors, etc.(Bumajdad et al., 2018; Sigwadi et al., 2019). Also, the high oxidoreductase ability of ZrO_2 allows for the maintenance of enhanced dielectric properties and so can be potential to serve as an insulator in transistors and portable hybrid electronic devices (Daunis et al., 2020; Öksüz et al., 2017. The applications of ZrO_2 can further be enhanced by creating more defective sites for oxygen at its crystal surface and one way to do so is by converting it into a smaller size of several nanometers. In that way, the nanoparticles (NPs) of ZrO_2 are very much suitable particularly for the applications of oxygen and nitrogen gas storage, optical sensors, optoelectronic, dielectric, and bioceramics (Doroshkevich et al., 2022; Zhang et al., 2020).

There are several synthesis routes for the formation of nanosized ZrO_2 that the method influences physicochemical properties such as bandgap energy, thermal stability, and porosity. In addition, synthesis parameters such as the method of manufacturing, reaction temperature, use of surfactants as sta-

bilizers, the extent of doping, etc. As the ZrO_2 NPs when they get fully stabilized by making use of external agents or ionic liquid stabilizers, the oxygen ion transporting ability and thermal resistivity gets multiplied, and thus formed composite structures are very much suitable in the high-temperature energy conversion devices and photonics (Farag et al., 2011).

In general, under normal atmospheric and temperature conditions, ZrO_2 exists in three different crystallographic forms, cubic (c-ZrO_2), tetragonal (t-ZrO_2), and monoclinic (m-ZrO_2) phases, where the mode of application dictates which polymorphic phase to be used. In addition to the three phases, another high-pressure allotropic form of ZrO_2, the orthorhombic phase has been reported and this form is metastable under atmospheric pressure conditions which readily revert to the monoclinic form (Itagaki et al., 2022). The m-ZrO_2 phase has stability up to 1100°C, while t-ZrO_2 is stable in the temperature range of 1100-2370°C, and the most stable c-ZrO_2 form can be found even at higher temperatures (>2370°C) (Nazir et al., 2021). For the synthesis of ZrO_2 NPs with varying phases, several techniques are being developed including the hydrolysis (Marković and Milonjić, 2006), sol-gel (Guel et al., 2017), spray pyrolysis (Waghmare et al., 2018), vapor phase(Moravec et al., 2007), pyrolysis (Hwangbo and Lee, 2019), microwave plasma (Vollath and Szabó, 2006), hydrothermal (Behbahani et al., 2012), co-precipitation (Mei et al., 2013), combustion (Dobrosz-Gomez et al., 2015), and ultrasonication (Guel et al., 2017). The combustion, co-precipitation, and microwave plasma routes generate highly porous c-ZrO_2 NPs having a well-organized morphology, while the sonochemical/ultrasonication method produces t-ZrO_2 and the hydrothermal, sol-gel, hydrolysis methods offer m-ZrO_2 NPs. In terms of applications, the c-ZrO_2 phase due to its stability (either directly or doped with Cu, Ni, and Co) over a range of temperatures and pressures covers a majority of sectors (fuel cells, catalysis, and sensors). On the other hand, the t-ZrO_2 phase exhibits superior electrical and mechanical properties that suit the low-temperature chemical engineering applications. The m-ZrO_2 phase has very attractive physicochemical properties and is commonly applied in ceramic-related products as pigments for the decoration of tiles, refractories, abrasive/piezoelectric/dielectric materials, coatings of thermal barriers, stones, glass, gems, etc (Farag et al., 2011).

Exploration of synthesis methods with simple and low-cost features will be advantageous for developing nanomaterials. A single monoclinic phase of ZrO_2 NPs was synthesized using a hydrothermal method. Whivh concluded that the variation in temperature and time of hydrothermal treatment influences the optical properties of the nanoparticles. Based on these studies, this research selected the optimum hydrothermal conditions with specific objectives for photocatalytic applications (Ahmad et al., 2017; Kumari et al., 2009; Sagadevan et al., 2016). In the present investigation, we employed one-pot hydrothermal synthesis for the formation of ZrO_2 NPs. To support the stability of photocatalytic activity, the calcination of the prepared nanoparticles is also an important factor (Jung and Park, 2001). The method applied in this research use the ideal condition, which is 200°C and 22 h, with additional calcination temperature of 200°C for 2 h. The formed ZrO_2 NPs were characterized for their crystallinity and crystal nature (by powder X-ray diffraction analysis), morphology (scanning electron microscopy), functionality and surface bonding (Fourier transform infrared and Raman), and optical properties (UV-Vis and fluorescence). In addition, the photocatalytic property of ZrO_2 NPs was examined in photooxidation of rhodamine B (RhB), which has not been reported previously. The results from this study are potential inputs for the development of industrial applications.

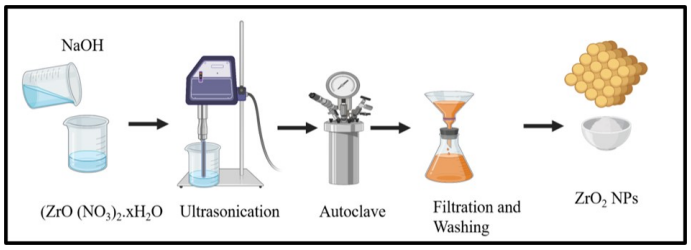

Figure 1. Schematic Representation of ZrO_2 NPs Formed by the Hydrothermal Synthesis Route

2. EXPERIMENTAL SECTION

2.1 Materials

ZrO_2 NPs were formed by the hydrothermal synthesis of zirconyl nitrate hydrate (ZrO $(NO_3)_2.xH_2O$) in the presence of sodium hydroxide (NaOH) (Sigma-Aldrich, Mumbai, India). The chemicals obtained were used in their original forms without any further modifications.

2.2 Synthesis of ZrO_2 NPs

To form ZrO_2 NPs, we first prepared individual stock solutions of ZrO $(NO_3)_2.xH_2O$ (0.5 M), and NaOH (5 M), with distilled water as the solvent. Equal volumes of both solutions were mixed under constant magnetic stirring, and furthermore the sonication for 30 min was applied until a homogeneous solution obtained. Approximately 10 mL of the solution mixture was hydrothermally treated in a 20 mL Teflon-lined autoclave with the addition of 2 mL of absolute ethanol. The treatment was at 200°C for 22 h, and afterward, the autoclave was made to cool to room temperature. Finally, the product was obtained and washed with deionized water several times until a neutral pH of 7 has been achieved. The dry white-colored powder of ZrO_2 NPs sample was obtained after that the obtained solid was kept in an oven at 80°C for 1h. A schematic representation of ZrO_2 NPs formation via the hydrothermal synthesis route is shown in Figure 1.

2.3 Instrumentation

The X-ray diffraction pattern of the sample was recorded on a Powder X-ray diffractometer using a Rigaku Smart Lab

(λ=1.54 A°). UV-DRS analysis was performed using a UV-visible spectrophotometer (Varian Technologies, USA). FT-IR and Raman studies were carried out using a Spectrum 100 FT-IR instrument (Perkin Elmer, USA) and Raman-11Nanophoton Corporation (Japan). Morphological studies using an FEI-Quanta FEG 200F instrument.

2.4 Photocatalytic Activity Test

Examination of the ZrO_2 NPs photocatalytic activity was performed for rhodamine B (RhB) degradation in a photocatalytic oxidation system. Typically, approximately 250 mL of RhB solution was placed in a water-jacket batch reactor equipped with a UV lamp (296 nm, 20 watt, 58.22 MW/cm^2). About 0.3 g of ZrO_2 NPs and 10^{-4} M of H_2O_2 were added and stirred for 15 min in the dark to achieve an adsorption equilibrium before light illumination. The sampling and analysis of RhB concentration were performed at certain time intervals. Colorimetric analysis of RhB was conducted using a UV-visible spectrophotometer (HITACHI U-2080). Photocatalysis, adsorption, and photolysis were performed as control experiments. Degradation efficiency (DE) was evaluated by comparing the concentrations of the initial and treated solutions using the following equation:

$$DE = \frac{[RhB]_0 - [RhB]_t}{[RhB]_0} \times 100$$

With $[RhB]_0$ and $[RhB]_t$ are RhB initial concentration and the concentration at time t, respectively.

3. RESULTS AND DISCUSSION

3.1 Physicochemical Character

The XRD patterns of the ZrO_2 NPs are shown in Figure 2. From the analysis, the ZrO_2 NPs have reflection patterns along the crystal planes of (111), (002), (022), (202), (113), (311), and (222), which can be attributed to the formation of the monoclinic phase of ZrO_2 according to JCPDS card no. 37-1484 (Hirvonen et al., 2006; Itagaki et al., 2022. In addition, there is no other peak detected, confirming the absence of impurities and high crystallinity. Such an observation of highly intense and well-organized peaks is only possible due to an increase in the crystalline planes of ZrO_2 associated with particle size enlargement (Hwangbo and Lee, 2019).

Figure 3 shows the FTIR spectrum of ZrO_2 NPs. The broad and sharp peaks situated at 3386 and 1630 cm^{-1} can be attributed to the -OH stretching and bending vibrations of adsorbed water molecules. The peak at 1135 cm^{-1} indicates the hydroxyl group of surface-adsorbed hydrated molecules (Liu et al., 2023). From the spectrum, the observation of a band at 485 cm^{-1} is attributed to Zr-O stretching vibration, while the band at 735 cm^{-1} is for the Zr-O bending vibration and thereby confirming the formation of ZrO_2 compound (Patel et al., 2017; Sigwadi et al., 2019). Further, to investigate the phase type of ZrO_2 (i.e., monoclinic, tetragonal, or cubic), Raman spectroscopy was performed and provided the result in

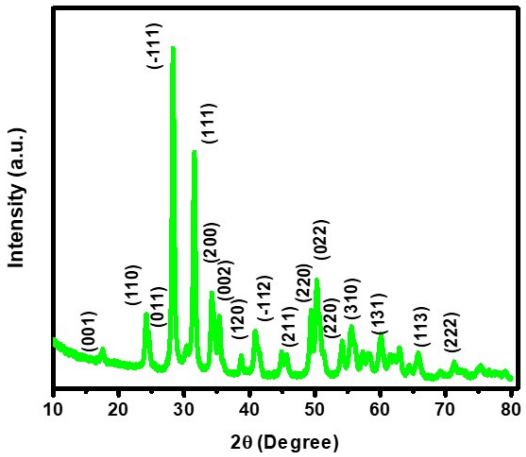

Figure 2. Powder XRD Patterns of ZrO_2 NPs

Figure 4. From the Raman spectral peaks analysis, the strong bands for the ZrO_2 sample are observed at 190, 335, and 476 cm^{-1}, in addition to several other bands. The same ZrO_2 sample from the literature studies (Basahel et al., 2015; Liu et al., 2023) has peaks majoring at 183, 335, and 476 cm^{-1} which indicates the availability of ZrO_2 in its dominant monoclinic phase. However, the other spectral peaks for the synthesized ZrO_2 sample, 222, 305, 385, 558, 615, 638, 675, 708, 955, 1018, and 1419 cm^{-1} corresponds to the tetragonal phase of ZrO_2 (Basahel et al., 2015). Therefore, from the cumulative analysis of all Raman spectral peaks, the as-synthesized ZrO_2 sample has mixed phases of both and with the major being for the monoclinic phase and the minor for the tetragonal were observed.

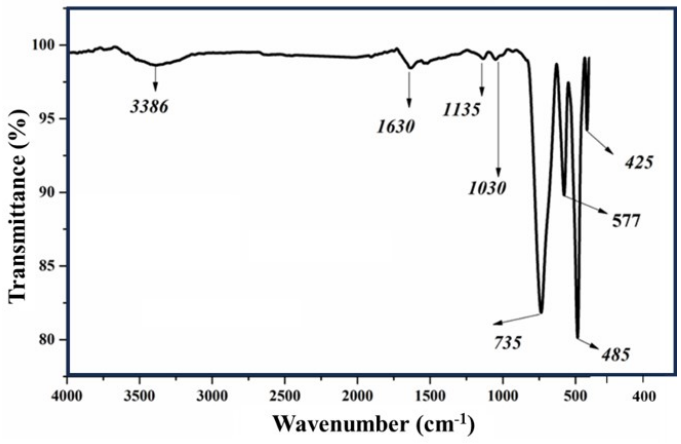

Figure 3. FTIR Spectral Analysis of ZrO_2 NPs

Figure 5(a-d) exhibits the SEM images of the ZrO_2 NPs at different magnifications. The SEM images show an aggregation or overlap of smaller-sized ZrO_2 particles to produce larger

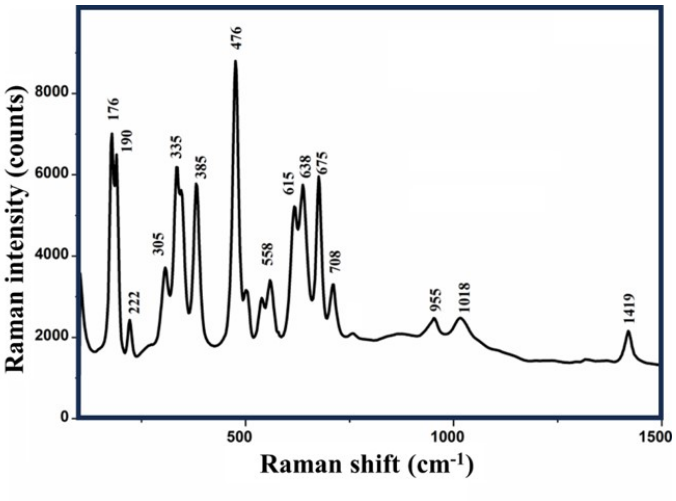

Figure 4. Raman Spectral Analysis of ZrO_2 NPs

ones. Agglomeration caused the varied-sized particles in the ZrO_2 particles to have an irregular structure, and from the SEM images, the grains appeared to be distributed randomly and appeared a spherical shape. Furthermore, the EDX spectra of the ZrO_2 NPs depicted in Figure 5(e) confirm the presence of Zr and O in the powdered sample.

It is a well-known fact that XPS is a very sensitive tool for the investigation of chemical states of various elements in a composite and so, we employed the XPS analysis for the understanding of Zr and its electronic state in the ZrO_2 NPs powder (Azdad et al., 2018; Srivastava et al., 2016). Figure 6 displays the XPS survey spectrum of the ZrO_2 that represents Zr 3d and O 1s spectra, indicating two main elements in the sample. From the graph, the peaks located at 181.3 and 183.8 eV can be attributed to the spin-orbit splitting of the Zr 3d component, where Zr $3d_{5/2}$ and Zr $3d_{3/2}$ are located at 181.98 and 184.29 eV respectively. Also, the binding energy of O 1s in ZrO_2 is located at 529.90 eV. The deconvolution of XPS of the Zr elemental peak indicates the availability of two different Zr species, i.e., one Zr^{2+} species observed with a low binding energy of 181.98 eV (monoclinic phase) and the other Zr^{4+} species having the high binding energy of 184.29 eV (tetragonal phase). Also, one thing to be noted for any ZrO_2 sample is that the fraction of Zr^{4+} species is significantly high as compared to the other Zr^{2+} species and the normal binding energy position for the Zr^{4+} species in pure ZrO_2 sample can be observed around 182.6 eV (Srivastava et al., 2016). In our case, the observation of a slightly lower binding energy value (181.98 eV) for m-ZrO_2 sample as compared to the stoichiometric ZrO_2 can be linked to the oxygen deficiency and associated holes generated by the oxygen vacancies in the lattice structure of ZrO_2 (Azdad et al., 2018). Accordingly, the surfaces of recovered ZrO_2 NPs are composed dominantly of Zr^{4+} and O^{2-} sites, in addition to some minor surface groups of -OH and -CO_x species, and adsorbed water molecules. The observed minor species (-OH, -CO_x, and H_2O) were also identified in

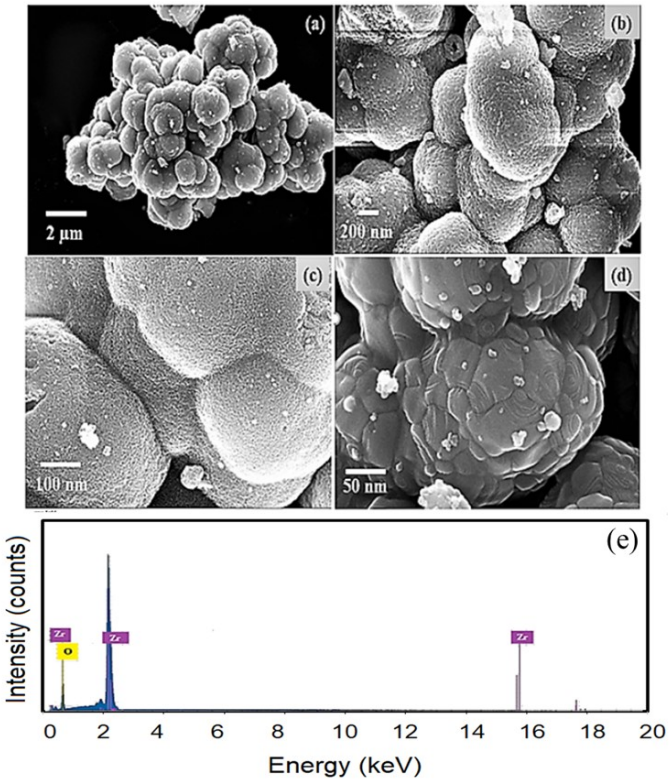

Figure 5. SEM Images at Different Magnifications (a-d) and EDX Spectrum (e) of ZrO_2 NPs

the FTIR spectrum of the ZrO_2 sample (Figure 3), thereby providing evidence for the exposure/adsorption of ZrO_2 NP's surface to the atmospheric gases rather maintaining chemically clean surfaces.

The most dynamic property of any NPs with respect to the size evolutions and concomitant structural changes commonly gets mapped in the optical absorption spectra and in that view, the UV-Vis absorption spectroscopy serves as an efficient technique for the monitoring of optical properties of quantum-sized particles. The UV-Vis absorbance of the ZrO_2 spectrum is shown in Figure 7, where the graph has two absorption maximums, one at 270 nm and another at 414 nm. Such an observation of the ZrO_2 sample's absorption maxima can be linked to the slight differences in the distribution of Zr^{4+} ions among many different sites of Zr-O, oxygen vacancies, and other structural defects (Azdad et al., 2018; Fatimah, 2014). However, in a similar study Li et al. (2007) the ZrO_2 NPs when available in m-ZrO_2 crystalline form have produced only a sharp absorption peak around 270 nm. Thus, the observation of absorption maxima for ZrO_2 samples in the range of 250 to 350 nm can be linked to the charge transfer transitions from $O_2 \rightarrow Zr^{4+}$ with Zr being in a low coordination state (mostly six) either in an isolated or available in the small Zr_xOy clusters (Azdad et al., 2018). The plotting of a graph between $(\alpha h\upsilon)^2$ and $h\upsilon$, and then extrapolating the line drawn tangent to the resulting curve gives the value of band gap energy, as shown in

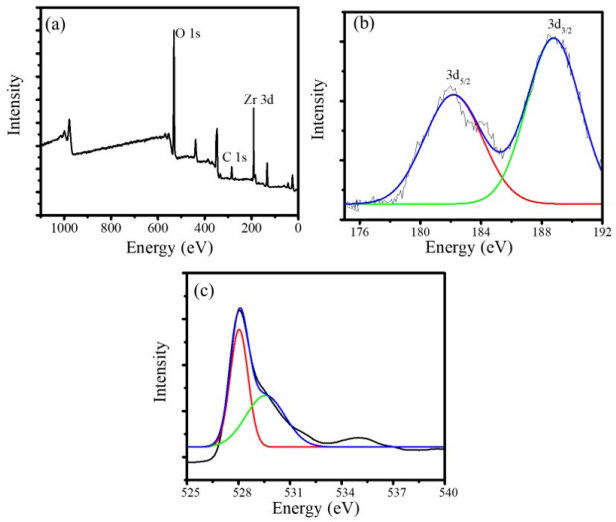

Figure 6. (a)Survey Scan Spectrum of ZrO_2 NPs, (b) Deconvolution of Zr 3d Spectrum, c. Deconvolution of O 1s Spectrum

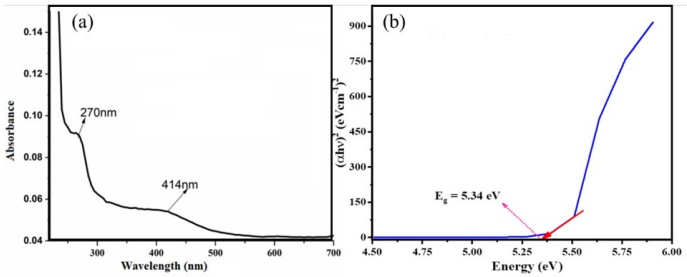

Figure 7. (a) UV-Vis Absorbance Spectrum and (b) the Corresponding Tauc's Plot of As-prepared ZrO_2 NPs

Figure 7(b). The optical direct band-gap energy (Eg) of ZrO_2 NPs was found to be 5.34 eV.

Similarly, Figure 8 provides the FL spectrum of ZrO_2 NPs where the graph summarizes the main photoluminescence (PL) transitions and are appearing due to some intrinsic defects discussed in the literature, i.e., based on the calculation of oxygen vacancies (Vo) energy level above the valence band (VB) (Bhaskar et al., 2020; Horti et al., 2020). In that way, the observation of an emission band for the ZrO_2 sample around 473 nm can be attributed to the transition of electrons among the two energy levels (oxygen vacancies and VB) and thereby suggesting a possible origin for the observation of blue emission. As discussed in the literature, a shift in the ZrO_2 sample's emission band towards a longer wavelength region was observed and this can be linked to the quantum size effect which originate from the reduced size of ZrO_2 particles. Thus, in our case, at the room temperature the increase of blue emission intensity is getting influenced strongly by the high crystal quality and quantum confinement effects of ZrO_2 nanostructures (Bhaskar

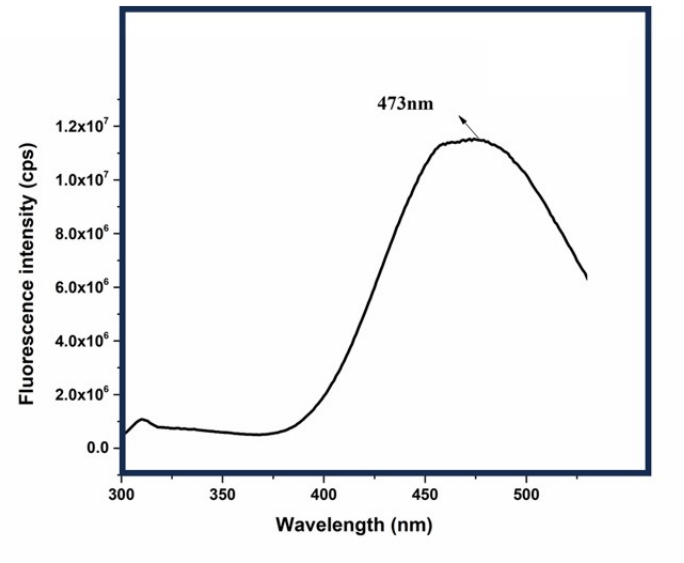

Figure 8. FL Emission Spectrum of ZrO_2 NPs

et al., 2020). Further, this decrease in FL intensity is due to the phase transition from tetragonal to tetragonal-monoclinic mixed-phase, and in addition, the shifting of FL peak towards the higher wavelength side is due to the reduction of grain size and electron trapping at oxygen vacancies. A similar kind of behaviour was also reported by Channu et al. (2011), i.e., the decreased FL intensity and shift in FL peak position are linked to the phase transition of ZrO_2 from monoclinic to the monoclinic-cubic mixed phase. Therefore, based on the analysis and comparison with literature studies, the present results point out that ZrO_2 NPs are maintaining the PL properties and their FL intensity is due to the oxygen vacancies and surface defects. This FL intensity can strongly be influenced by changing the crystallinity and quantum confinement effects, where this phenomenon suits well for the applications of light-emitting diodes and photo-electronic devices.

3.2 Photocatalytic Activity Examination

The photocatalytic activity of the prepared ZrO_2 was examined for the photocatalytic oxidation of RhB. For this process, H_2O_2 was used as an additional oxidant in the system. Figure 9 shows the kinetics of RhB degradation of the prepared photocatalyst; to ensure the activity, the adsorption process, photocatalytic, and photolytic treatments were also assessed. The adsorption was treated with ZrO_2 addition without any light or oxidant, whereas the photocatalytic treatment was conducted in the presence of ZrO_2 addition with light but without any oxidant. In addition, a photolytic treatment was used to evaluate the effect of UV light on possible degradation. As can be seen from the kinetics plots, photocatalytic oxidation exhibited the highest degradation rate, as approximately 89% of RhB was degraded within 2 h. The comparison curves revealed the initial degradation rate in the following order: photocatalytic oxidation > photocatalytic > adsorption> photolytic. These results sug-

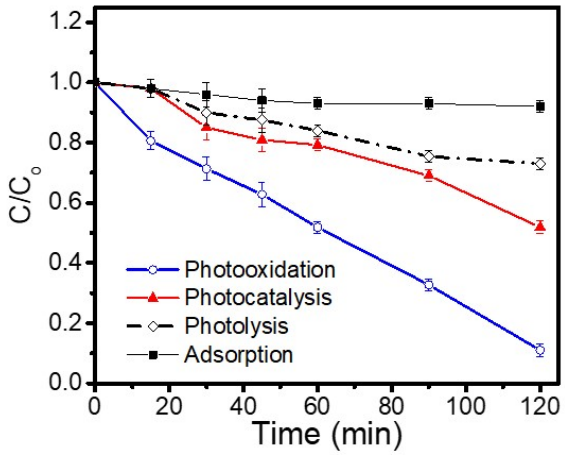

Figure 9. Kinetics of RhB Degradation by Varied Treatment Over Prepared ZrO_2 NPs

gest that ZrO_2 acts as a photocatalyst, and H_2O_2 and UV light synergistically affect the degradation mechanism. Without a photocatalyst, the exposed light could not produce oxidant species to further oxidize RhB as a target molecule. In different mechanisms, adsorption reduces the RhB concentration on the specific surface of ZrO_2. By means of the provided photon source and H_2O_2 as oxidant, homolytic cleavage could be processed, and the interaction between •OH radicals with the solvent and O_2 produced the reactive oxidant species (Fatimah et al., 2022). In summary, the prepared ZrO_2 exhibited photocatalytic activity, which is consistent with its physicochemical features.

Referring to the degradation efficiency, the activity of the prepared ZrO_2 NPs was comparable to that of other ZrO_2-based photocatalysts. As an example, the degradation efficiency in this work is higher than that reported by sol-gel synthesized ZrO_2 Wang et al. (2023) which showed 60% degradation efficiency, with respect to that reported by Padovini et al. (2019) who demonstrated a degradation efficiency of less than 10% in the photocatalytic treatment of RhB. These results imply that ZrO_2 prepared using the method described in this work is a promising nanomaterial.

3.3 Effect of pH on Photocatalytic Activity

To evaluate the effect of photocatalysis on the pH of the aqueous environment, a study on the effect of pH on photocatalytic activity was performed within the range of 4-11. As shown in Figure 10a, the initial rate of the photocatalytic reaction as a function of pH is optimum at neutral pH = 9. The effect of pH on photocatalytic activity is related to the zeta potential of the ZrO_2 NPs. From Figure 10b, it can be seen that the zeta potential was 0.206 mV with a standard deviation of 1.59 mV, which is relatively stable under neutral pH leading to acidic conditions. The adsorption of RhB dye by the photocatalyst

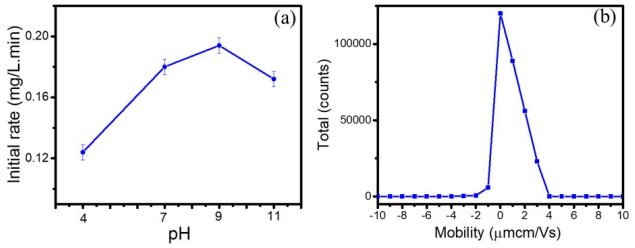

Figure 10. (a) Effect of pH on Initial Rate of Reaction (b) Zeta Potential Measurement of ZrO_2 NPs

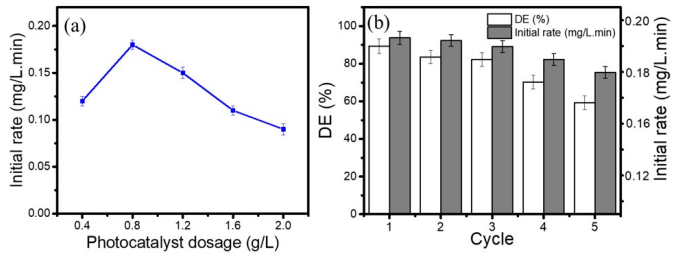

Figure 11. (a) Effect of Photocatalyst Dosage on Initial Rate and DE of Reaction (b) Reusability of Photocatalyst

surface is a crucial factor that influences the surface mechanism during photocatalysis since the electrostatic interactions of surface with RhB will determine the effectiveness of surface reaction and propagation steps (Andreas and Oktaviani, 2022; Leong et al., 2022). Under acidic conditions, the presence of the radical •OH is diminished by the provided H^+, and the propagation of oxidation is inhibited. Moreover, the electrostatic repulsion was higher than that under alkaline conditions. In contrast, under alkaline conditions, the provided hydroxyl supports the formation of an oxidizing agent in the solution, but under very basic conditions, the abundant hydroxyl terminates the propagation. This phenomenon is similar to that reported for RhB oxidation over WO_3, Polyaniline (PANI)/TiO_2 and CdS/TiO_2, which is related to the surface properties of the photocatalyst (Andreas and Oktaviani, 2022; Laatar et al., 2017; Mzimela et al., 2022).

3.4 Effect of Photocatalyst Dosage

Photocatalyst dosage is a key factor affecting the degradation efficiency of the photocatalytic oxidation mechanism. Figure 11a shows the initial rate of RhB degradation at varying photocatalyst loadings (0.4 g/L to 2 g/L) at an initial RhB concentration of 10 ppm and a pH of 9. As can be seen from the plot, the optimum condition was reached by the dosage of 1.2 g/L, after which the initial rate decreased significantly up to 2 g/L. Turbidity is the most likely condition for inhibiting light penetration into the solution. Consequently, decreasing the number of photons reduces the number of hydroxyl radicals formed in the system (Mzimela et al., 2022).

3.5 Reusability of Photocatalyst

The reusability profile of ZrO_2 NPs as a photocatalyst was evaluated by measuring the DE and the initial rate of reaction in five cycles. Recycling was performed by filtering the nanoparticle powder, followed by washing with ethanol and drying at a temperature of 80°C in an oven. The bar presented in Figure 11b indicates that the material is stable until 3^{rd} cycle as the changes in DE and the initial rate are not significant. Further recycling resulted in a lower DE and initial rate, representing the loss of photocatalytic activity. Referring to previous works on the study of reusability, the most possible factor for decreasing activity is the surface blocking by the adsorbed dye (Vinayagam et al., 2022).

4. CONCLUSION

In summary, (ZrO_2) nanostructures were prepared using a one-pot hydrothermal route and studied the crystallinity, morphology, surface functionality, and optical properties. From the powder XRD analysis, the as-synthesized zirconia was found to be of pure monoclinic phase (m-ZrO_2). The SEM indicated that the spherical morphology of the particles aggregated to form larger particles. FTIR and Raman spectral analyses demonstrated the strong presence of ZrO_2 NPs. In addition, the XPS analysis of the formed ZrO_2 nanopowder with in-depth analysis of Zr 3d and O 1s elements highlights the pure crystals with well-organized electronic states for Zr and O atoms. In addition, XPS studies confirmed the availability of zirconia suboxides and oxygen defects/vacancies in theZrO_2 nanostructures. Finally, the ZrO_2 NPs showed photocatalytic activity comparable to that of other related materials. The study showed that the pH and photocatalyst dosage significantly influenced the degradation efficiency and initial rate, as shown by the optimum conditions of pH 9 and a dosage of 0.8 g/L, respectively. The ZrO_2 NPs exhibited photocatalyst stability for three cycles of usage, after which deactivation was identified by the reduced degradation efficiency and initial rate of reaction.

5. ACKNOWLEDGMENT

The authors are grateful to the University of Malaya for funding this work under grant number MG020-2022.

REFERENCES

Ahmad, T., M. Shahazad, and R. Phul (2017). Hydrothermal Synthesis, Characterization and Dielectric Properties of Zirconia Nanoparticles. *Material Science and Engineering International Journal*, **1**; 100–104

Andreas, R. and A. Oktaviani (2022). Synthesis, Characterization, and Activity of The Photocatalyst Polyaniline (PANI)/TiO2 in Degrading Rhodamine B Dye. *Science and Technology Indonesia*, **7**(1); 126–131

Azdad, Z., L. Marot, L. Moser, R. Steiner, and E. Meyer (2018). Valence Band Behaviour of Zirconium Oxide, Photoelectron and Auger Spectroscopy Study. *Scientific Reports*, **8**(1); 16251

Basahel, S. N., T. T. Ali, M. Mokhtar, and K. Narasimharao (2015). Influence of Crystal Structure of Nanosized ZrO_2 on Photocatalytic Degradation of Methyl Orange. *Nanoscale Research Letters*, **10**; 1–13

Behbahani, A., S. Rowshanzamir, and A. Esmaeilifar (2012). Hydrothermal Synthesis of Zirconia Nanoparticles from Commercial Zirconia. *Procedia Engineering*, **42**; 908–917

Bhaskar, S., E. W. Awin, K. H. Kumar, A. Lale, S. Bernard, and R. Kumar (2020). Design of Nanoscaled Heterojunctions in Precursor-derived t-ZrO_2/SiOC (N) Nanocomposites: Transgressing the Boundaries of Catalytic Activity from UV to Visible Light. *Scientific Reports*, **10**(1); 430

Bumajdad, A., A. A. Nazeer, F. Al Sagheer, S. Nahar, and M. I. Zaki (2018). Controlled Synthesis of ZrO_2 Nanoparticles with Tailored Size, Morphology and Crystal Phases via Organic/inorganic Hybrid Films. *Scientific Reports*, **8**(1); 3695

Channu, V. R., R. R. Kalluru, M. Schlesinger, M. Mehring, and R. Holze (2011). Synthesis and Characterization of ZrO_2 Nanoparticles for Optical and Electrochemical Applications. *Colloids and Surfaces A: Physicochemical and Engineering Aspects*, **386**(1-3); 151–157

Daunis, T. B., K. A. Schroder, and J. W. Hsu (2020). Photonic Curing of Solution-deposited ZrO_2 Dielectric on PEN: a Path Towards High-throughput Processing of Oxide Electronics. *npj Flexible Electronics*, **4**(1); 7

Dobrosz-Gomez, I., M. Á. Gómez-García, J. Bojarska, M. Kozanecki, and J. M. Rynkowski (2015). Combustion Synthesis and Properties of Nanocrystalline Zirconium Oxide. *Comptes Rendus Chimie*, **18**(10); 1094–1105

Doroshkevich, A. S., A. I. Lyubchyk, B. L. Oksengendler, T. Y. Zelenyak, N. O. Appazov, A. K. Kirillov, T. A. Vasilenko, A. A. Tatarinova, O. O. Gorban, and V. I. Bodnarchuk (2022). Electric Energy Storage Effect in Hydrated ZrO_2-Nanostructured System. *Nanomaterials*, **12**(11); 1783

Farag, H. K., K. H. Hegab, and S. Zein El Abedin (2011). Preparation and Characterization of Zirconia and Mixed Zirconia/titania in Ionic Liquids. *Journal of Materials Science*, **46**; 3330–3336

Fatimah, I. (2014). Preparation of ZrO_2/Al_2O_3-Montmorillonite Composite as Catalyst for Phenol Hydroxylation. *Journal of Advanced Research*, **5**(6); 663–670

Fatimah, I., G. Purwiandono, I. Sahroni, S. Sagadevan, W. Chun-Oh, S. A. I. S. M. Ghazali, and R.-a. Doong (2022). Recyclable Catalyst of ZnO/SiO_2 Prepared from Salacca Leaves Ash for Sustainable Biodiesel Conversion. *South African Journal of Chemical Engineering*, **40**(1); 134–143

Guel, M. L. A., L. D. Jiménez, and D. A. C. Hernández (2017). Ultrasound-Assisted Sol-gel Synthesis of ZrO_2. *Ultrasonics Sonochemistry*, **35**; 514–517

Hirvonen, A., R. Nowak, Y. Yamamoto, T. Sekino, and K. Niihara (2006). Fabrication, Structure, Mechanical and Thermal Properties of Zirconia-based Ceramic Nanocomposites.

Journal of the European Ceramic Society, **26**(8); 1497–1505
Horti, N., M. Kamatagi, S. Nataraj, M. Wari, and S. Inamdar (2020). Structural and Optical Properties of Zirconium Oxide (ZrO_2) Nanoparticles: Effect of Calcination Temperature. *Nano Express*, **1**(1); 010022
Hwangbo, Y. and Y. I. Lee (2019). Facile Synthesis of Zirconia Nanoparticles Using a Salt-assisted Ultrasonic Spray Pyrolysis Combined with a Citrate Precursor Method. *Journal of Alloys and Compounds*, **771**; 821–826
Itagaki, Y., M. Takemoto, H. Murata, T. Kanzawa, Y. Tokudome, and A. Nakahira (2022). Supercritical Hydrothermal Synthesis of Zirconia Nanoparticles from Zirconium Basic Carbonate. *Journal of the Ceramic Society of Japan*, **130**(11); 861–866
Jung, K. Y. and S. B. Park (2001). Effect of Calcination Temperature and Addition of Silica, Zirconia, Alumina on the Photocatalytic Activity of Titania. *Korean Journal of Chemical Engineering*, **18**; 879–888
Kumari, L., W. Li, J. Xu, R. Leblanc, D. Wang, Y. Li, H. Guo, and J. Zhang (2009). Controlled Hydrothermal Synthesis of Zirconium Oxide Nanostructures and their Optical Properties. *Crystal Growth and Design*, **9**(9); 3874–3880
Laatar, F., H. Moussa, H. Alem, L. Balan, E. Girot, G. Medjahdi, H. Ezzaouia, and R. Schneider (2017). CdSe Nanorod/TiO_2 Nanoparticle Heterojunctions with Enhanced Solar-and Visible-light Photocatalytic Activity. *Beilstein Journal of Nanotechnology*, **8**(1); 2741–2752
Lebeau, B., I. Naboulsi, L. Michelin, C. Marichal, S. Rigolet, C. Carteret, S. Brunet, M. Bonne, and J.-L. Blin (2020). Amorphous Mesostructured Zirconia with High (Hydro) Thermal Stability. *RSC Advances*, **10**(44); 26165–26176
Leong, C. Y., H. L. Teh, M. C. Chen, and S. L. Lee (2022). Effect of Synthesis Methods on Properties of Copper Oxide Doped Titanium Dioxide Photocatalyst in Dye Photodegradation of Rhodamine B. *Science and Technology Indonesia*, **7**(1); 91–97
Li, J., S. Meng, J. Niu, and H. Lu (2017). Electronic Structures and Optical Properties of Monoclinic ZrO_2 Studied by First-principles Local Density Approximation+ U Approach. *Journal of Advanced Ceramics*, **6**; 43–49
Li, N., B. Dong, W. Yuan, Y. Gao, L. Zheng, Y. Huang, and S. Wang (2007). ZrO_2 Nanoparticles Synthesized Using Ionic Liquid Microemulsion. *Journal of Dispersion Science and Technology*, **28**(7); 1030–1033
Liu, S., J. Wang, Y. Chen, Z. Song, B. Han, H. Wu, T. Zhang, and M. Liu (2023). Tetragonal Nanosized Zirconia: Hydrothermal Synthesis and Its Performance as a Promising Ceramic Reinforcement. *Inorganics*, **11**(5); 217
Marković, J. P. and S. K. Milonjić (2006). Synthesis of Zirconia Colloidal Dispersions by Forced Hydrolysis. *Journal of the Serbian Chemical Society*, **71**(6); 613–619
Mei, Y., C. Meisheng, N. Zhang, L. Zhiqi, and X. Huang (2013). Characterization of CeO_2-ZrO_2 Mixed Oxides Prepared by Two Different Co-precipitation Methods. *Journal of Rare Earths*, **31**(3); 251–256
Moravec, P., J. Smolík, H. Keskinen, J. M. Mäkelä, V. V. Levdansky, et al. (2007). Vapor Phase Synthesis of Zirconia Fine Particles from Zirconium Tetra-tert-butoxide. *Aerosol and Air Quality Research*, **7**(4); 563–577
Mzimela, N., S. Tichapondwa, and E. Chirwa (2022). Visible-Light-Activated Photocatalytic Degradation of Rhodamine B Using WO_3 Nanoparticles. *RSC Advances*, **12**(53); 34652–34659
Nazir, M. A., T. Mahmood, A. A. Zafar, N. Akhtar, T. Hussain, M. A. Saeed, F.-e. Aleem, A. Saeed, J. Raza, and C. Cao (2021). Electronic, Optical and Elastic Properties of Cubic Zirconia (c-ZrO_2) Under Pressure: A DFT Study. *Physica B: Condensed Matter*, **604**; 412462
Öksüz, K., Ş. Şen, and U. Şen (2017). Influence of ZrO_2 Addition on the Structure and Dielectric Properties of BaTiO3 Ceramics. *Acta Physica Polonica A*, **131**(1); 197–199
Padovini, D., A. Magdalena, R. Capeli, E. Longo, C. Dalmaschio, A. Chiquito, and F. Pontes (2019). Synthesis and Characterization of ZrO_2@SiO_2 Core-shell Nanostructure as Nanocatalyst: Application for Environmental Remediation of Rhodamine B Dye Aqueous Solution. *Materials Chemistry and Physics*, **233**; 1–8
Patel, S. B., N. Baker, I. Marques, A. Hamlekhan, M. T. Mathew, C. Takoudis, C. Friedrich, C. Sukotjo, and T. Shokuhfar (2017). Transparent TiO_2 Nanotubes on Zirconia for Biomedical Applications. *RSC Advances*, **7**(48); 30397–30410
Sagadevan, S., J. Podder, and I. Das (2016). Hydrothermal Synthesis of Zirconium Oxide Nanoparticles and Its Characterization. *Journal of Materials Science: Materials in Electronics*, **27**; 5622–5627
Sigwadi, R., M. Dhlamini, T. Mokrani, and F. Nemavhola (2019). Preparation of a High Surface Area Zirconium Oxide for Fuel Cell Application. *International Journal of Mechanical and Materials Engineering*, **14**(1); 1–11
Srivastava, M., P. Bera, J. Balaraju, and B. Ravisankar (2016). FESEM and XPS Studies of ZrO_2 Modified Electrodeposited NiCoCrAlY Nanocomposite Coating Subjected to Hot Corrosion Environment. *RSC Advances*, **6**(110); 109083–109090
Tran, T. V., D. T. C. Nguyen, P. S. Kumar, A. T. M. Din, A. A. Jalil, and D. V. N. Vo (2022). Green Synthesis of ZrO_2 Nanoparticles and Nanocomposites for Biomedical and Environmental Applications: A Review. *Environmental Chemistry Letters*, **20**(2); 1–23
Vinayagam, R., B. Singhania, G. Murugesan, P. S. Kumar, R. Bhole, M. K. Narasimhan, T. Varadavenkatesan, and R. Selvaraj (2022). Photocatalytic Degradation of Methylene Blue Dye Using Newly Synthesized Zirconia Nanoparticles. *Environmental Research*, **214**; 113785
Vollath, D. and D. V. Szabó (2006). The Microwave Plasma Process–a Versatile Process to Synthesise Nanoparticulate Materials. *Journal of Nanoparticle Research*, **8**; 417–428
Waghmare, M., P. Sonone, P. Patil, V. Kadam, H. Pathan, and A. Ubale (2018). Spray Pyrolytic Deposition of Zirconium

Oxide Thin Films: Influence of Concentration on Structural and Optical Properties. *Engineered Science*, **5**(2); 79–87

Wang, J., R. Yu, Z. Li, F. Yang, L. Luo, D. Wang, H. Cheng, Y. Zhang, and Q. Zhang (2023). Heteropolyacid-loaded MOF-derived Mesoporous Zirconia Catalyst for Chemical Degradation of Rhodamine B. *Green Processing and Synthesis*, **12**(1); 20230005

Zhang, L., S. Dorjpalam, G. Ji, and J. Peng (2020). Corrosion of Stainless Steel Coated with a ZrO_2 Film in a Hydrogen Sulfide Gas Environment. *SN Applied Sciences*, **2**; 1–12

